International Journal of Heat and Mass Transfer 52 (2009) 4883–4893

Contents lists available at ScienceDirect

International Journal of Heat and Mass Transfer

journal homepage: www.elsevier.com/locate/ijhmt

An experimental study in determining the local heat transfer coefficients for the plate finned-tube heat exchangers

Cheng-Hung Huang [a,*], I-Cha Yuan [a], Herchang Ay [b]

[a] Department of Systems and Naval Mechatronic Engineering, National Cheng Kung University, Tainan 701, Taiwan, ROC
[b] Department of Mold and Die Engineering, National Kaohsiung University of Applied Sciences, Kaohsiung 807, Taiwan, ROC

ARTICLE INFO

Article history:
Received 13 November 2008
Received in revised form 14 May 2009
Accepted 14 May 2009
Available online 9 July 2009

Keywords:
Inverse problem
Heat transfer coefficients determination
Plate finned-tube heat exchangers

ABSTRACT

A three-dimensional inverse problem in determining the local heat transfer coefficients for the plate finned-tube heat exchangers utilizing the steepest descent method (SDM) and a general purpose commercial code CFX4.4 is applied successfully in the present study based on the measured temperature distributions on fin surface by infrared thermography.

Two different tube arrangements (i.e. in-line and staggered) with different fin pitch and air velocity are considered and the corresponding local heat transfer coefficients are to be determined. Results show that some interesting phenomena of the local heat transfer coefficients for the finned surface are found in the work and the averaged heat transfer coefficient of the staggered configuration is about 8–13% higher than that of the in-line configuration.

1. Introduction

Finned surfaces of the plate finned-tube heat exchangers have been in use over a long period of time for dissipation of heat by convection. Applications for finned surfaces are widely seen in air-conditioning, electrical, chemical, refrigeration, cryogenics and many cooling systems in industrial. Kays and London [1] introduced various types of heat transfer surfaces.

For the purpose of energy savings, it is important to design better heat transfer surfaces such that high efficient heat transfer equipment can be obtained. To achieve this goal, the estimation of local convective heat transfer coefficients for fin surface becomes importance in designing the high-performance heat exchangers. However, the estimation of the convective heat transfer coefficient is more difficult to perform than other common thermo-fluid-dynamic quantities, especially in case of non-uniform distributions and/or of conduction–convection problem.

In recent years, an infrared thermographic system has developed as an effective tool for measurement of surface temperature distribution and for heat flux restoration due to its high spatial and temporal resolution, high sensitivity, and noninvasive nature. For instantance, Cardone et al. [2] examined the flow produced by a flat disk rotating in still air by an infrared camera. Henckels et al. [3] and Simeonides et al. [4] applied the infrared thermographic technique to measure the heat transfer in a hypersonic tunnel. Ay [5] and Ay and Yang [6] used an infrared thermovision to visualize the real-time thermal-image processing in the global temperature distribution over the surfaces of the cutting tool, workpiece and chip.

Available experimental information on the plate fin and tube heat exchangers have been presented, reviewed and correlated in the open literatures. Rich [7,8] examined the effects of fin-pitch and number of tube row for staggered plate fin and tube heat exchangers. Saboya and Sparrow [9–11] applied the naphthalene mass transfer method to measure the local coefficients for one to three rows, plate-fin and tube heat exchangers. A lot of the experimental data has been collected in a book by McQusiston [12].

Recently, Ay et al. [13] used energy balance method and infrared thermography to estimate the local convective heat transfer coefficients of finned surfaces for the two-dimensional plate finned-tube heat exchangers. The results show that the dominant heat transfer coefficients occurred at the leading edge of plate-fin and between first row tubes. Huang et al. [14] applied the technique of steepest descent method (SDM) in the three-dimensional plate finned-tube heat exchangers to estimate the unknown local heat transfer coefficients and obtained good estimations. In [14] they devised an inverse algorithm, which has the ability to communicate with the commercial code CFX4.4 by means of data transportation, and a 3-D inverse heat conduction problem for plate finned-tube heat exchangers was established and used to estimate the local convective heat transfer coefficient. Only numerical experiments were performed in [14], no experiments were conducted.

Yan et al. [15] applied the transient liquid crystal thermograph technique to examine the effects of surface-mounted obstacles on

* Corresponding author. Tel.: +886 6 2747018; fax: +886 6 2747019.
E-mail address: chhuang@mail.ncku.edu.tw (C.-H. Huang).

0017-9310/$ - see front matter © 2009 Elsevier Ltd. All rights reserved.
doi:10.1016/j.ijheatmasstransfer.2009.05.023

Nomenclature

$h(S_{f5})$, $h(S_{f6})$	local heat transfer coefficient
$J[h(S_{fi})]$	functional defined by Eq. (2)
$J'[h(S_{fi})]$	gradient of functional defined by Eq. (8)
k	thermal conductivity
M	total number of measured temperature extracting points
$P(S_{fi})$	direction of descent defined by Eq. (4)
q	boundary heat flux
S_f	fin surface
$T(\Omega)$	estimated temperature
$\Delta T(\Omega)$	sensitivity function defined by Eq. (5)
$Y(S_{fi})$	measured temperature

Greek letters

β	search step size
$\lambda(\Omega)$	Lagrange multiplier defined by Eq. (7)
$\Omega=(x,y,z)$	fin domain

Superscript

n	iteration index

the local heat transfer enhancement of a base plate. The results show that when the obstacles (i.e. the tubes in this study) are protruded in the main stream, the horse-shoe (HS) vortex formed in front of the obstacle–plate junction strongly enhances the local heat transfer. Therefore, the dominant heat transfer coefficients of this study occurred in front of obstacles (or tubes).

The conclusions of [13,15] are not consistent, to make a detail examination, the present study is to utilize same experimental technique as [13] (i.e. advanced infrared thermovision system), but different estimating algorithm, i.e. the technique of steepest descent method (SDM) [14], to estimate the local convective heat transfer coefficients of finned surfaces for the three-dimensional plate finned-tube heat exchangers.

Two different tube arrangements (i.e. in-line and staggered) with different fin pitch and air velocity will be considered and the corresponding local heat transfer coefficients are to be determined. The steepest descent method has great potential in solving three-dimensional inverse problems [16–19]. It derives basis from the perturbational principles [20] and transforms the inverse problem to the solution of three problems, namely, the direct problem, the sensitivity problem and the adjoint problem, which will be briefly discussed in the following sections.

2. Direct problem

The test models for the in-line and staggered plate finned-tube heat exchangers are shown in Fig. 1. To develop the methodology for use in determining the local convective heat transfer coefficients on the fin surface, the following three-dimensional inverse heat conduction problem is considered.

The mathematical formulation of this problem is similar to the work by Huang et al. [14], the only difference is the applied boundary conditions on the tube surfaces. In [13], the tube boundary surfaces are subjected to a prescribed temperature condition, but this becomes difficult to achieve in any real experiments with air cooling. For this reason the boundary conditions on tube surfaces are taken as a prescribed heat flux condition in this work. Electric power is supplied to the heater through cables from a GW GPS-3030 DC power supply (0–30 V, 0–3 A) to generate the heat flux in the experiments.

Finally the direct problem becomes

$$\frac{\partial^2 T(\Omega)}{\partial x^2}+\frac{\partial^2 T(\Omega)}{\partial y^2}+\frac{\partial^2 T(\Omega)}{\partial z^2}=0; \quad \text{in } \Omega(x,y,z) \tag{1a}$$

$$\frac{\partial T(S_{fi})}{\partial n}=0; \quad \text{on fin side surfaces } S_{fi}\ i=1\text{–}4 \tag{1b}$$

$$-k\frac{\partial T(S_{f5})}{\partial z}=h(S_{f5})(T_\infty-T); \quad \text{on fin top surface } S_{f5} \tag{1c}$$

$$-k\frac{\partial T(S_{f6})}{\partial z}=h(S_{f6})(T-T_\infty); \quad \text{on fin bottom surface } S_{f6} \tag{1d}$$

$$-k\frac{\partial T(S_{\mathrm{ti}})}{\partial z}=q_i; \quad \text{on tube surfaces} \tag{1e}$$

The direct problem considered here is concerned with calculating the plate fin temperatures when the heat transfer coefficient $h(S_{fi})$, $i=5$ and 6, thermal conductivity and boundary condition on tube surfaces are known. The solution for the above 3-D heat conduction problem in domain Ω is solved using CFX4.4 [21] and its Fortran subroutine USRBCS.

3. The inverse problem

For the inverse problem, the local heat transfer coefficients $h(S_i)$, $i=5$ and 6, are regarded as being unknown, but everything else in Eq. (1) is known. In addition, the temperature readings using infrared thermography on the fin surface S_5 and S_6 are assumed available. The fin thickness is very thin in this work and it is reasonable to assume that $T(S_{f5})=T(S_{f6})$ and $h(S_{f5})=h(S_{f6})$ for the present study.

Let the temperature reading taken by infrared scanners on fin surfaces S_5 and S_6 be denoted by $\mathbf{Y}(S_{fi})\equiv Y(x_m,y_m)\equiv Y_m(S_{fi})$, $m=1$–M and $i=5$ and 6, where M represents the number of measured temperature extracting points. We note that the measured temperature $Y_m(S_{fi})$ should contain measurement errors. The inverse problem can be stated as follows: by utilizing the above mentioned measured temperature data $Y_m(S_{fi})$, estimate the unknown local heat transfer coefficient $h(S_{fi})$, $i=5$ and 6.

The solution of the present inverse problem is to be obtained in such a way that the following functional is minimized:

$$J[h(S_{fi})]=\sum_{m=1}^{M}[T_m(S_{fi})-Y_m(S_{fi})]^2; \quad i=5 \quad \text{and} \quad 6 \tag{2}$$

Here, $T_m(S_{fi})$ is the estimated or computed temperatures at the measured temperature extracting locations (x_m,y_m). These quantities are determined from the solution of the direct problem given previously by using the estimated local heat transfer coefficient $h(S_{fi})$.

4. Steepest descent method for minimization

The following iterative process based on the steepest descent method [14] is now used for the estimation of unknown heat transfer coefficient $h(S_{fi})$ by minimizing the functional $J[h(S_{fi})]$:

$$h^{n+1}(S_{fi})=h^n(S_{fi})-\beta^n P^n(S_{fi}); \quad \text{for } n=0,1,2,\ldots \text{ and } i=5,6 \tag{3}$$

where β^n is the search step size in going from iteration n to iteration $n+1$, and $P^n(S_{fi})$ is the direction of descent (i.e. search direction) given by

$$P^n(S_{fi})=J'^n(S_{fi}); \quad i=5 \quad \text{and} \quad 6 \tag{4}$$

which is identical to the gradient direction $J'^n(S_{fi})$ at iteration n.

To perform the iterations according to Eq. (4), we need to compute the step size β^n and the gradient of the functional $J'^n(S_{fi})$. In order to develop expressions for the determination of these two

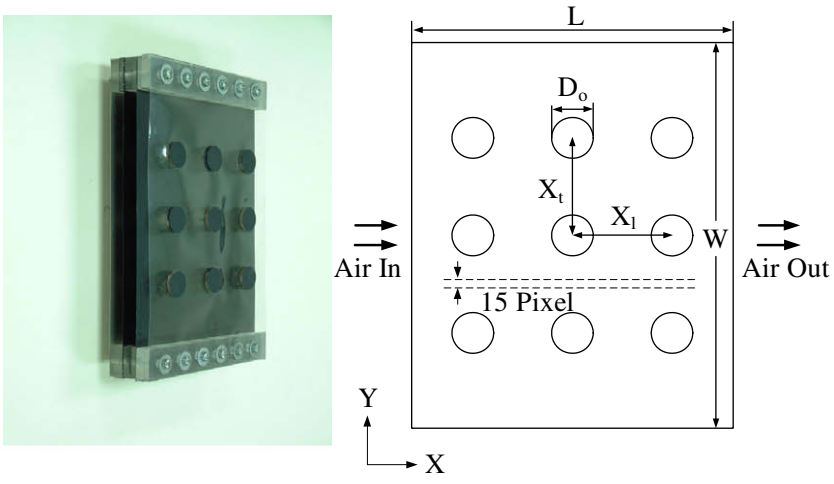

Fig. 1. The finned-tube heat exchangers of the present study in the (a) in-line arrangement and (b) staggered arrangement.

quantities, a "sensitivity problem" and an "adjoint problem" are constructed as described below.

4.1. Sensitivity problem and search step size

By following the standard procedure as [14], the following sensitivity problems for the sensitivity function ΔT is obtained:

$$\frac{\partial^2 \Delta T(\Omega)}{\partial x^2}+\frac{\partial^2 \Delta T(\Omega)}{\partial y^2}+\frac{\partial^2 \Delta T(\Omega)}{\partial z^2}=0; \quad \text{in } \Omega(x,y,z) \tag{5a}$$

$$\frac{\partial \Delta T(S_{fi})}{\partial n}=0; \quad \text{on fin side surfaces } S_{fi},\ i=1\text{–}4 \tag{5b}$$

$$-h\Delta T+k\frac{\partial \Delta T}{\partial z}=\Delta h(T-T_\infty); \quad \text{on fin top surface } S_{f5} \tag{5c}$$

$$h\Delta T+k\frac{\partial \Delta T}{\partial z}=\Delta h(T_\infty-T); \quad \text{on fin bottom surface } S_{f6} \tag{5d}$$

$$\frac{\partial \Delta T}{\partial n}=0; \quad \text{on tube surfaces} \tag{5e}$$

CFX 4.4 is used to solve above sensitivity problem.

The search step size β^n can also be determined by the following expression:

$$\beta^n=\frac{\sum_{m=1}^{M}[T_m(S_{fi})-Y_m(S_{fi})]\Delta T_m(S_{fi})}{\sum_{m=1}^{M}[\Delta T_m(S_{fi})]^2}; \quad i=5 \quad \text{and} \quad 6 \tag{6}$$

4.2. Adjoint problem and gradient equation

By following the standard procedure as [14], the following adjoint problem for determining $\lambda(\Omega)$ can be obtained:

$$\frac{\partial^2 \lambda(\Omega)}{\partial x^2}+\frac{\partial^2 \lambda(\Omega)}{\partial y^2}+\frac{\partial^2 \lambda(\Omega)}{\partial z^2}=0; \quad \text{in } \Omega(x,y,z) \tag{7a}$$

$$\frac{\partial \lambda(S_{fi})}{\partial n}=0; \quad \text{on fin side surfaces } S_{fi},\ i=1\text{–}4 \tag{7b}$$

$$-\lambda h+k\frac{\partial \lambda}{\partial n}=2k[T(S_{f5})-Y(S_{f5})]\delta(x-x_m)\delta(y-y_m); \quad \text{on fin top surface } S_{f5} \tag{7c}$$

$$\lambda h+k\frac{\partial \lambda}{\partial n}=2k[T(S_{f6})-Y(S_{f6})]\delta(x-x_m)\delta(y-y_m); \quad \text{on fin bottom surface } S_{f6} \tag{7d}$$

$$\frac{\partial\lambda(S_{ti})}{\partial n}=0; \quad \text{on tube surfaces} \tag{7e}$$

Finally, the following expression for the gradient of the functional $J[h(S_{fi})]$ can be obtained:

$$J'[h(S_{fi})]=\frac{\lambda(S_{fi})}{k}[T(S_{fi})-T_\infty]; \quad \text{on surfaces } S_{fi},\ i=5 \text{ and } 6 \tag{8}$$

5. Experimental equipments and procedure

The experimental setup and equipments are basically similar to those were used in [13], for this reason we have just described briefly here. Fig. 1 illustrated schematically the systems that were used to estimate the local heat transfer coefficients of a plate which consisted of a three-row plate fin and tube heat exchanger situated in a subsonic blow-down open-circuit wind tunnel.

The test section is the same as that used in [13] and is constructed of stainless steel for large scale testing of a bank of tubes shared continuous plate fins. Both of in-line and staggered tube arrangements are used in this study. For the description of coordinate systems and nomenclature for the tested fins, please refer to Fig. 2 in [13]. There are four different staggered and in-line test sections for the present experimental investigation, their detailed geometrical parameters are tabulated in Table 1 and also shown in Fig. 1. Each tube is locally heated by means of energy dissipation in a wire inserted in the central region of a cylinder installed in the tube. Electric power is supplied to the heater through cables from a GW GPS-3030 DC power supply (0–30 V, 0–3 A) to simulate the applied boundary heat flux. The surface of the fin is coated on both sides with thin film of opaque paint with emissivity ε of 0.95. In order to measure the temperature distribution on the surface of plate-fin inside test core by an infrared camera, a transparent sheet replaces the top plate-fin of the test core.

The experimental apparatus for infrared temperature measurements used is AGEMA Thermovision 550, THV550. The sensing system of THV550 is a focal plane array, FPA, detector made of a matrix with 320 (H) × 240 (V) PtSi elements.

For testing, the fan was started. The desired air velocity through the test section was set by means of adjusting an inverter. The frontal air velocity, U, was measured by a hot wire with ±2.0% accuracy. The power supplies were turned on and adjusted to serve as the boundary heat fluxes of the tubes. These heat fluxes can be calculated by recording the values of voltage and current of each tube. When steady-state values had been established, the temperature map of the plate-fin surface was recorded. The imaging size of the map was a plane matrix array with 220 pixels × 220 pixels for in-line and 194 pixels × 246 pixels for staggered arrangements.

Following the temperature value identified at each pixel by the infrared thermovision system, the local convective heat transfer coefficients over the fin can be determined by means of the above mentioned technique of inverse problem, i.e. the SDM.

Table 1
Geometrical parameters of the test sections.

Tube arrangement	In-line		Staggered	
Test section	1	2	3	4
Fin pitch, fp (mm)	10	15	10	15
Fin length, L (mm)	196		196	
Fin width, W (mm)	240		240	
Outer diameter of tube, D_0 (mm)	25.4		25.4	
Transverse pitch of tube, X_l (mm)	60.7		52.6	
Longitudinal pitch of tube, X_t (mm)	60.7		60.7	
Tube thickness, t_u (mm)	2.0		2.0	
Fin thickness, t_f (mm)	1		1	
Tube number	9		11	
Row number	3		3	

6. Results and discussions

The objective of the present study is to apply the SDM in estimating the local surface convective heat transfer coefficients for the three-dimensional plate finned-tube heat exchangers based on the measured temperature distributions on fin surface by infrared thermography. The physical model for this problem is described as follows: The thermal conductivity for plate fin is taken as k = 43 W/(m^2-K), ambient temperature is chosen as T_∞ = 300 K and the heat fluxes on each tube surface are given in Table 2. The grid systems of the fin are shown in Fig. 2, which represents the in-line and staggered tube arrangements for a fin plate.

Table 2
The surface heat fluxes of the tubes for the (a) in-line and (b) staggered arrangements with different fin pitch.

No.	Current (A)	Voltage (V)	Power (W)	Current (A)	Voltage (V)	Power (W)
(a) In-line arrangement (fp = 10 mm)				In-line arrangement (fp = 15 mm)		
1	0.55	5.00	2.75	0.55	5.00	2.75
2	0.55	4.60	2.53	0.50	4.90	2.45
3	0.62	5.00	3.10	0.58	5.10	2.96
4	0.55	4.80	2.64	0.51	4.50	2.30
5	0.50	4.00	2.00	0.48	4.20	2.02
6	0.50	4.00	2.00	0.50	4.90	2.45
7	0.55	5.00	2.75	0.60	5.00	3.00
8	0.50	4.00	2.00	0.52	4.80	2.50
9	0.50	5.00	2.50	0.55	5.20	2.86
(b) Staggered arrangement (fp = 10 mm)				Staggered arrangement (fp = 15 mm)		
1	1.30	3.40	4.42	1.25	3.20	4.00
2	0.50	4.40	2.20	0.55	5.00	2.75
3	0.55	4.40	2.42	0.59	5.00	2.95
4	1.21	3.90	4.72	1.30	3.50	4.55
5	0.50	4.00	2.00	0.49	4.50	2.21
6	0.55	4.50	2.48	0.42	3.80	1.60
7	0.48	4.00	1.92	0.55	5.00	2.75
8	1.30	3.20	4.16	1.12	2.80	3.14
9	0.50	4.00	2.00	0.50	4.50	2.25
10	0.45	4.00	1.80	0.50	4.50	2.25
11	1.20	3.50	4.20	1.15	3.80	4.37

One of the advantages of using the SDM is that the initial guesses of the unknown convective heat transfer coefficients $h(S_i)$ can be chosen arbitrarily. In all the cases considered here, the initial guesses of heat transfer coefficients used to begin the iteration are taken as $h(S_{fi}) = 0.0$.

The estimations in determining $h(S_{fi})$ by the inverse analysis are given below:

6.1. In-line arrangement

The dimension for fin in x-, y- and z-directions is 196 mm, 240 mm and 1 mm, respectively. The outer radius of tube is taken as 12.7 mm and the longitudinal pitch of tube (i.e. the distance between centers of two tubes) is 60.7 mm. The grid system for the present study is shown in Fig. 2(a). The grid in z-direction is taken as 5 and the total grid number on x–y-plane is 2940, therefore there are totally 14,700 grids in the present study.

The results of the infrared thermovision for steady-state temperature distribution on the plate-fin surface using frontal velocity $U = 0.5$ m/s for two different fin pitch $fp = 10$ and 15 mm are presented in Fig. 3.

By setting number of iteration equals 30 for both $fp = 10$ and 15 mm, the inverse solutions can be converged. The estimated (or calculated) fin surface temperature and estimated heat transfer coefficients are shown in Figs. 4 and 5, respectively. It can be seen from Figs. 3 and 4 that the calculated temperatures match measured temperatures very well, this implies that the estimated heat transfer coefficients should be correct. Besides when fin pitch is increased, the fin surface temperatures decrease and therefore heat transfer coefficients increase.

When comparing the measured temperatures of Fig. 3 in this study with Fig. 5(a) in [13], it can be found that the tendency is the same. However, the tendency for the estimated heat transfer coefficients is not similar even thought the order of magnitude is about the same. The results of the estimated heat transfer coefficients in [13] indicated that the dominant heat transfer coefficients occurred at the leading edge of plate-fin and between the adjacent areas of the first row tubes. However, the results in this work reveal that the dominant heat transfer coefficients are located in front of the first row tubes, i.e. tube numbers 1, 2 and 3 in Fig. 2(a).

Yan et al. [15] used the transient liquid crystal thermograph technique to examine the effects of surface-mounted obstacles on the local convective heat transfer enhancement of a base plate. They indicated that when the obstacles are protruded in the main stream, the horse-shoe (HS) vortex formed in front of the obstacle–plate junction strongly enhances the local heat transfer. Therefore, the dominant heat transfer coefficients of their study occurred in front of obstacles. Besides, they also concluded that as the obstacle height increases, the horse shoe vortex effect becomes stronger in the head-on stagnation region and therefore heat transfer coefficient increases.

The fin tubes of the present study can be treated as the circular obstacles in the study of Yan et al. [15] and therefore it is expected that the maximum heat transfer coefficient will occur in front of the fin tubes at the first row. Moreover, the larger fin pitch implies that the obstacle height increases and it is also expected that the larger the fin pitch, the higher the convective heat transfer coefficients in front of the fin tubes at the first row for a fixed air velocity.

Let us examine the estimated heat transfer coefficients in Fig. 5, it is obvious that for both fin pitches the maximum heat transfer coefficients did appear in front of the fin tubes at the first row and when the fin pitch increases, the heat transfer coefficients also

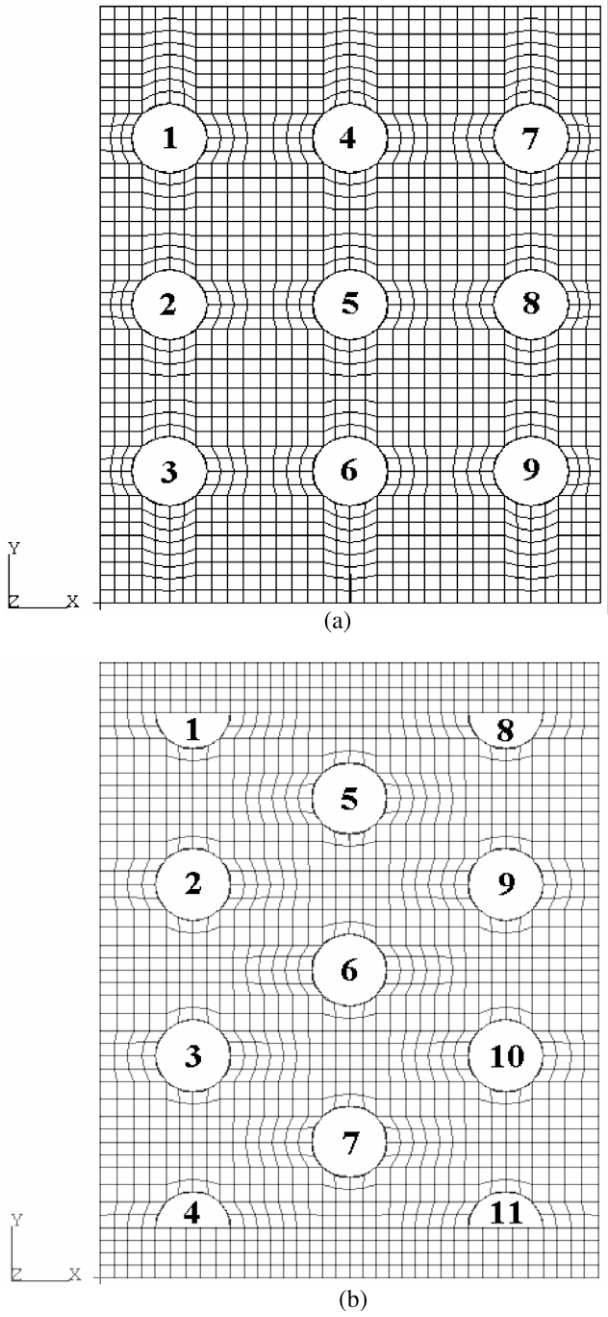

Fig. 2. The grid system for the (a) in-line and (b) staggered tube arrangements.

increase. One of the reasons is stated by Yan et al. [15] and the other one may be due to the fact that when the distance between fins is increased, air may move more freely between them and therefore increase the heat transfer coefficients.

The heat transfer coefficients become quite uniformly in the area between rear surfaces of the first row tubes and front surfaces of the last row tubes. Due to the turbulent and exit effects, heat transfer coefficients increase in the rear area of the last row tubes. This phenomenon becomes pronounced as the fin pitch increases.

Next the frontal velocity U is increased to 1.0 m/s and then to 1.5 m/s and two different fin pitch $fp = 10$ and 15 mm are also considered. The measured temperature distributions on plate-fin surface by the infrared thermovision at $U = 1.5$ m/s for $fp = 10$

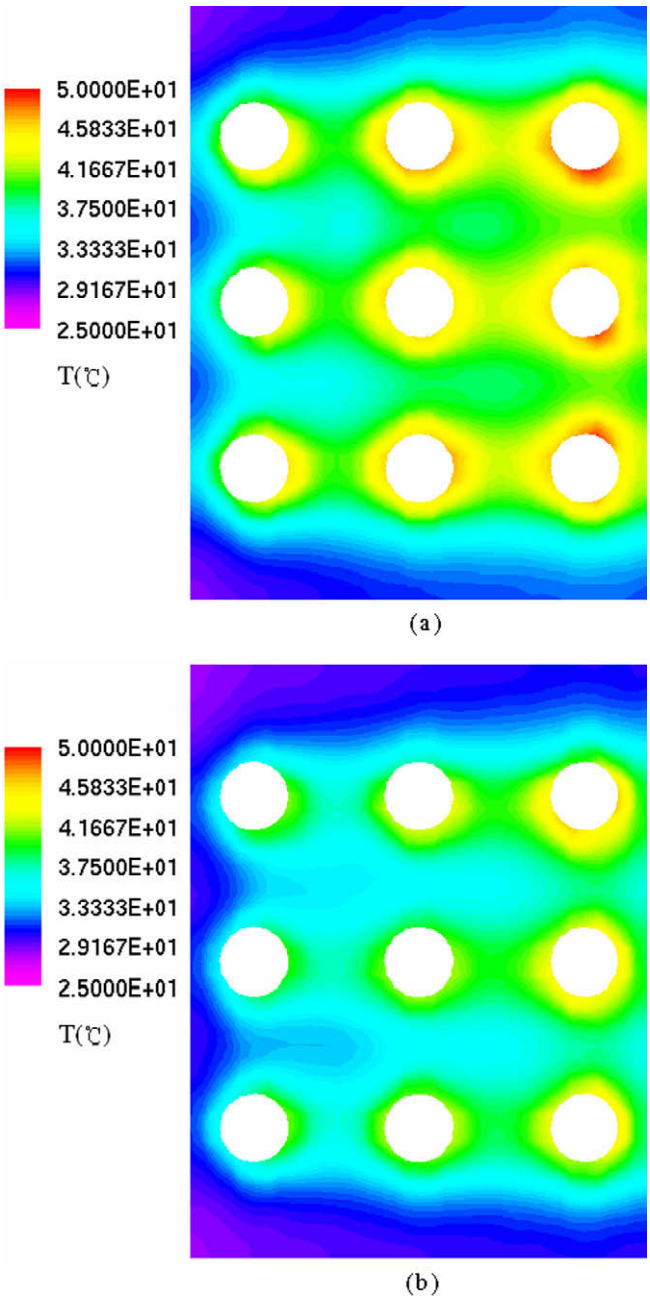

Fig. 3. The measured temperature distributions for the in-line arrangement using U = 0.5 m/s with (a) fp = 10 mm and (b) fp = 15 mm.

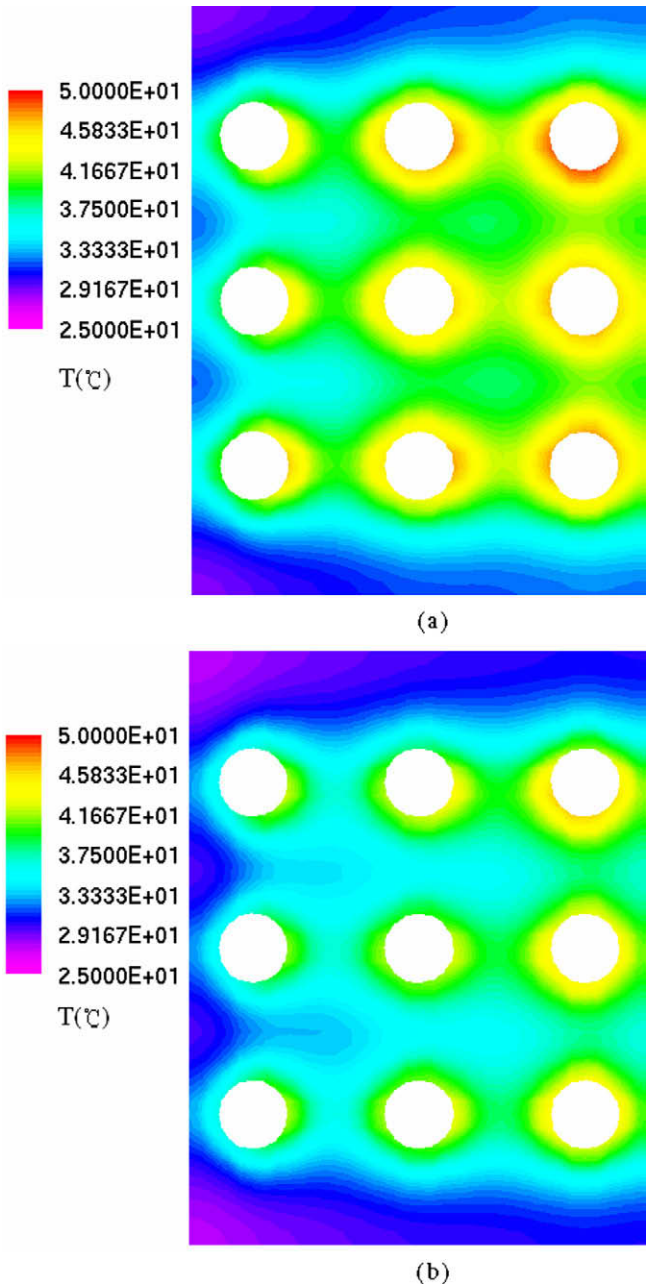

Fig. 4. The estimated temperature distributions for the in-line arrangement using U = 0.5 m/s with (a) fp = 10 mm and (b) fp = 15 mm.

and 15 mm are shown in Fig. 6. After 30 iterations for both cases the inverse solutions converged, Figs. 7 and 8 indicate the estimated (or calculated) fin surface temperatures and estimated heat transfer coefficients, respectively. Again the measured and estimated temperatures fit perfectly and this is one of the guarantees of accurate estimations. As expected, when air velocity increases the surface temperatures decrease and the heat transfer coefficients increase.

By comparing Fig. 3(a) with Fig. 6(a) and Fig. 3(b) with Fig. 6(b), it is found that the thermal layer in front of the first low tubes becomes thinner when air velocity is increased. This implies that larger heat transfer coefficient must be resulted to out come these phenomena. Indeed, by comparing Fig. 5(a) with Fig. 8(a) and Fig. 5(b) with Fig. 8(b), the effects of horse shoe vortex become stronger to result in a higher heat transfer coefficient in front of the first row tubes.

Another interesting phenomenon is that when considering U = 1.5 m/s and fp = 15 mm, the heat transfer coefficients around the second and third row tubes increased and became a circular shape. This is because for flows at higher velocity, larger velocity gradient in boundary layer and streamwise pressure gradient of on-coming flow result in a stronger horse shoe vortex in front of the tubes. The high velocity also leads to a strong forced convection effect on reattachment process. Therefore, heat transfer enhancement increases around the tubes with the increasing air velocity. Besides, due to the turbulent and exit effects, heat transfer coefficients also increase in the rear area of the last row tubes, these

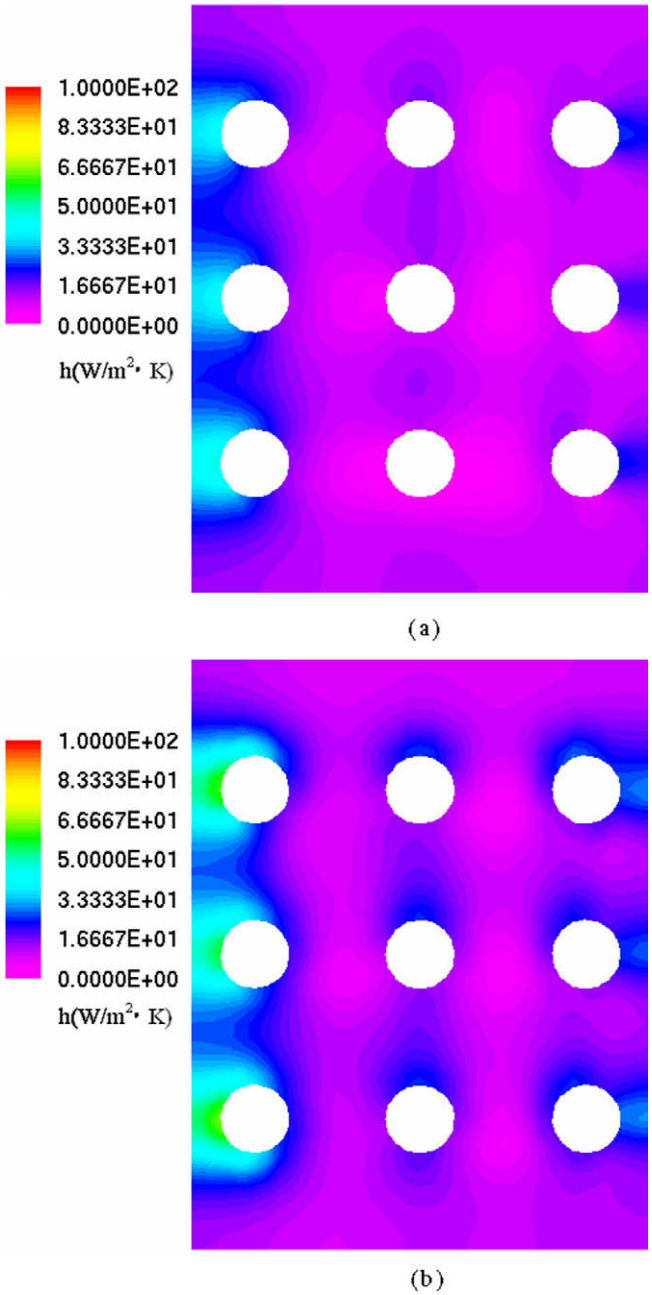

Fig. 5. The estimated heat transfer coefficients for the in-line arrangement using U = 0.5 m/s with (a) fp = 10 mm and (b) fp = 15 mm.

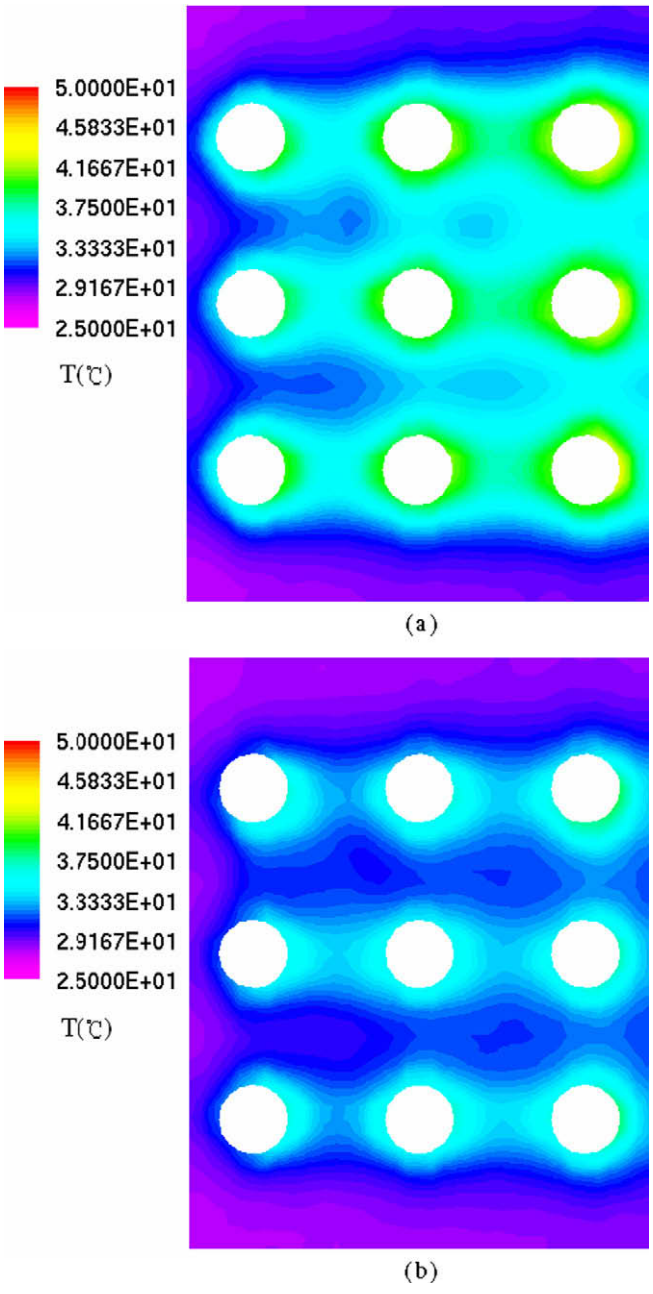

Fig. 6. The measured temperature distributions for the in-line arrangement using U = 1.5 m/s with (a) fp = 10 mm and (b) fp = 15 mm.

phenomena becomes more pronounced with increasing of air velocity and fin pitch.

6.2. Staggered arrangement

The dimensions for fins with staggered tube arrangement are reported in Table 1. The temperature distributions on the plate-fin surface by infrared thermovision using frontal velocity U = 0.5 m/s for two different fin pitch fp = 10 and 15 mm are presented in Fig. 9.

By setting number of iteration equal to 30 for both fp = 10 and 15 mm, the inverse solutions converged. The relative error between the measured and estimated fin surface temperatures is very small, this implies that the pictures will be similar and therefore the figures for the estimated temperatures are not shown here. The estimated heat transfer coefficients are shown in Fig. 10.

The tendency of the measured temperatures in Fig. 9(a) is similar to Fig. 5(b) in [13], but the tendency for the estimated heat transfer coefficients is again different even thought the order of magnitude is also similar. The results of the estimated heat transfer coefficients in [13] for the staggered arrangement is similar to that for the in-line arrangement in [13], but Fig. 10 reveals that the maximum heat transfer coefficients are located in front of the first row full tubes (number 2 and number 3 tubes in Fig. 2(b)) for the reasons stated before, also the dominant heat transfer coefficients exist at the up and down sides of the upper (number 1 tube in Fig. 2(b)) and lower (number 4 tube in Fig. 2(b)) half

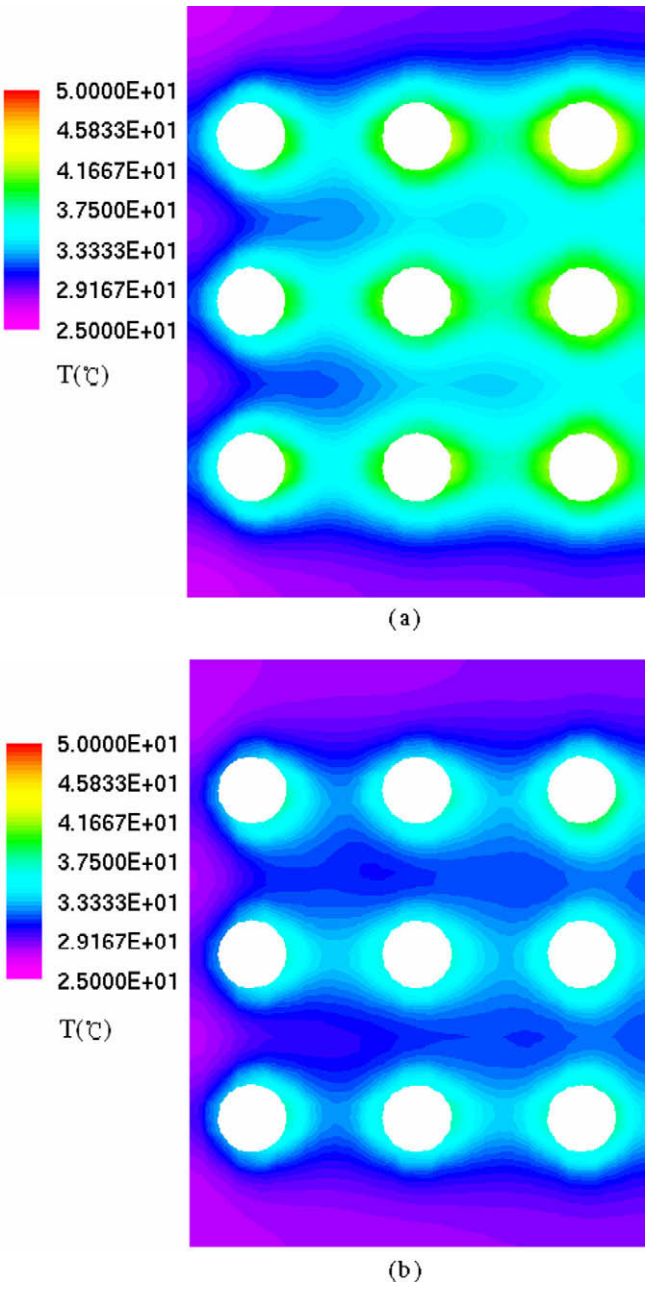

Fig. 7. The estimated temperature distributions for the in-line arrangement using U = 1.5 m/s with (a) fp = 10 mm and (b) fp = 15 mm.

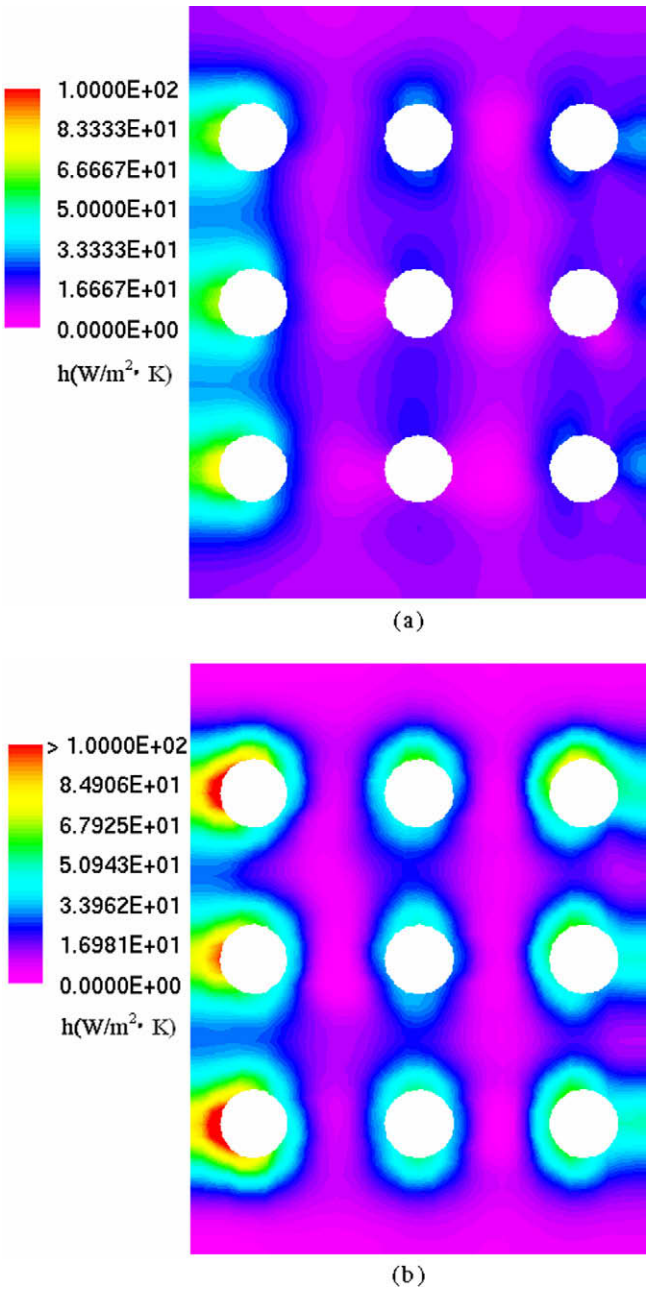

Fig. 8. The estimated heat transfer coefficients for the in-line arrangement using U = 1.5 m/s with (a) fp = 10 mm and (b) fp = 15 mm.

tubes, respectively. The reason for this is because air can flow freely through the flat surface of the upper and lower half tubes, this fact combines with the entrance effects will result in such a dominant heat transfer coefficient. The present tendency of the estimated heat transfer coefficients has not been found in [13].

The air velocity U is increased to 1.0 m/s and then to 1.5 m/s for two different fin pitch fp = 10 and 15 mm. The measured temperature distributions on plate-fin surface by the infrared thermovision for U = 1.5 m/s, fp = 10 and 15 mm are shown in Fig. 11. After 30 iterations for both cases the inverse solutions converged. Only the estimated heat transfer coefficients are shown in Fig. 12 since the estimated temperatures are very close to the measured temperatures. As air velocity increases, the surface temperatures decrease and heat transfer coefficients increase.

It is observed from Fig. 12 that the heat transfer coefficients around the second and third row tubes increased and formed a circular shape with lower air velocity and smaller fin pitch. As air velocity and fin pitch are increased, this phenomena becomes more pronounced. This has also been seen for the in-line arrangement but only for higher air velocity and larger fin pitch. For this reason it can be concluded easily that the performance for the staggered arrangement is better than that for the in-line arrangement.

From the above experimental test cases, the averaged heat transfer coefficients, $\bar{h}$, as well as the relative errors between the measured and estimated temperatures for the in-line and the staggered arrangements are all reported in Table 3. From Table 3 we learned that for a fixed tube arrangement, the larger the air velocity and fin pitch, the higher the convective heat transfer coefficient.

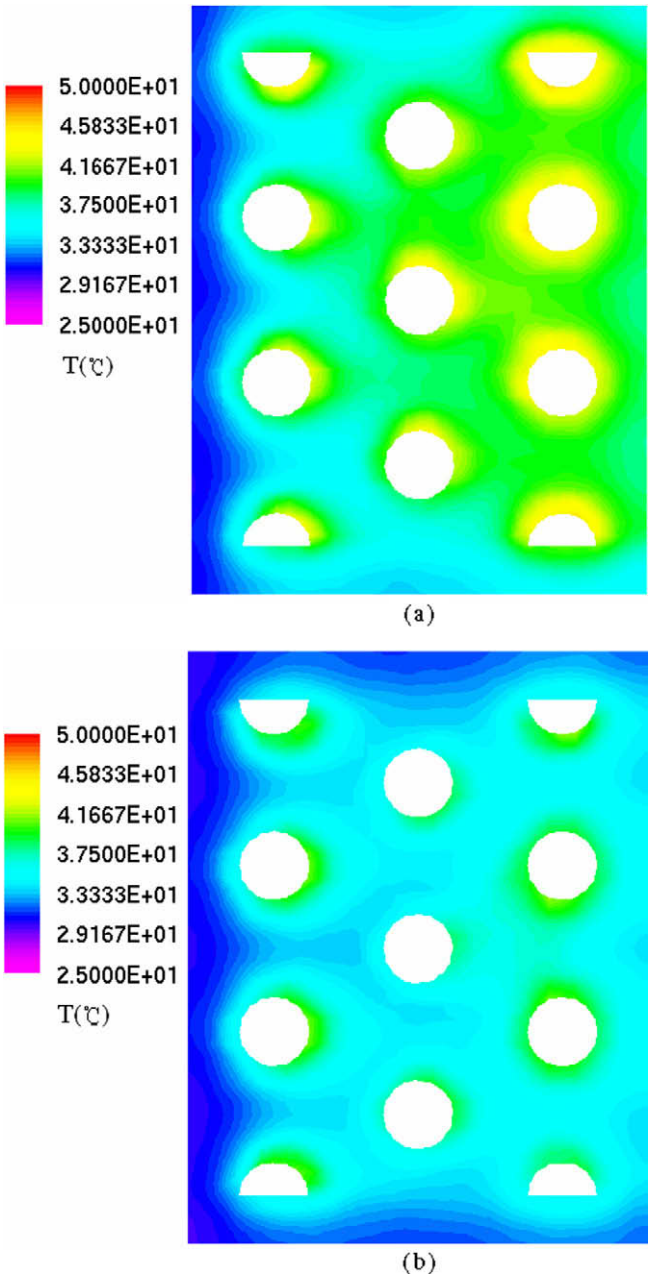

Fig. 9. The measured temperature distributions for the staggered arrangement using U = 0.5 m/s with (a) fp = 10 mm and (b) fp = 15 mm.

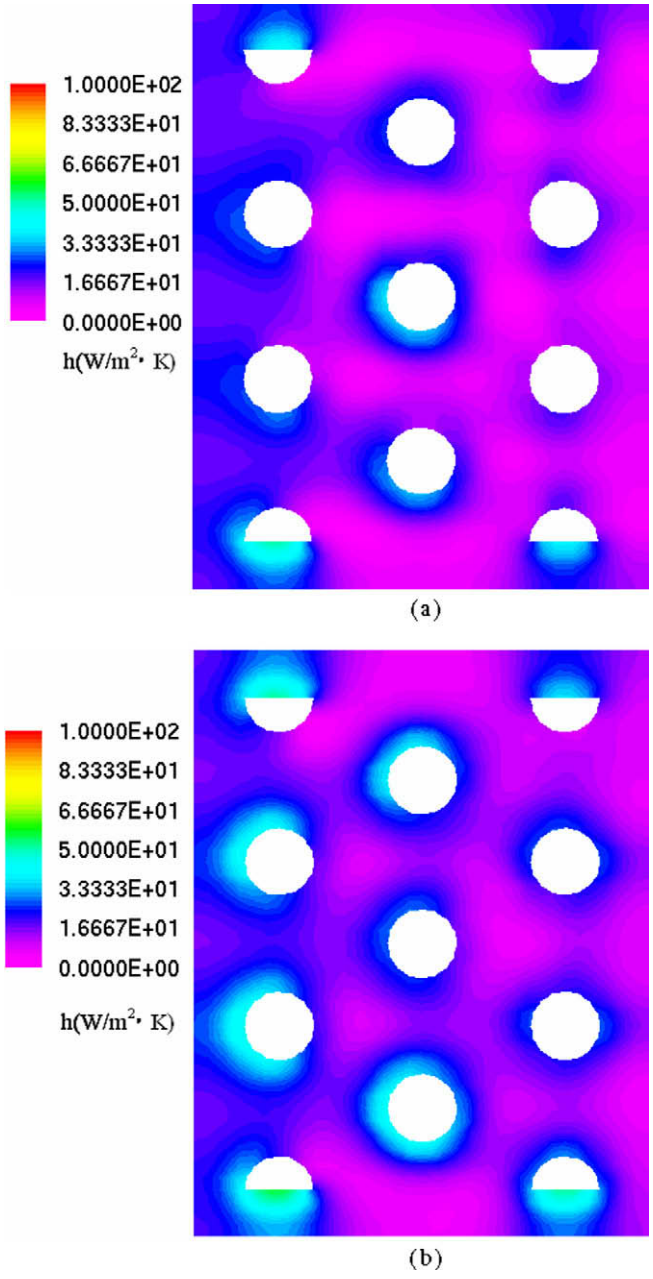

Fig. 10. The estimated heat transfer coefficients for the staggered arrangement using U = 0.5 m/s with (a) fp = 10 mm and (b) fp = 15 mm.

For the fixed air velocity and fin pitch, the convective heat transfer coefficient for the staggered arrangement is always better than that for the in-line tube arrangement.

In accordance with Fig. 12 in [13], they concluded that for the fixed fin pitch and air velocity, the heat transfer coefficient for the staggered arrangement is higher than that for the in-line arrangement, this is the same as our conclusions.

However, Fig. 12 in [13] also reported that for the fixed air velocity and tube arrangement, the larger the fin pitch, the smaller the convective heat transfer coefficient. This may not be true and may be due to the improper estimation model for estimating the convective heat transfer coefficient in [13] since when fin pitch is increased more free air will flow through the fin surfaces and lower fin temperatures will be resulted. As long as the temperature distribution on fin surface for larger fin pitch is lower than that for smaller fin pitch as shown in Figs. 3, 6, 9 and 11, the estimated heat transfer coefficients must be higher for the case with larger fin pitch arrangement.

Finally, it can be concluded that the steepest descent method is now applied successfully in this three-dimensional inverse heat conduction problem for predicting the surface heat transfer coefficients of plate fin.

7. Conclusions

A three-dimensional inverse heat conduction problem in estimating the local heat transfer coefficients for plate finned-tube

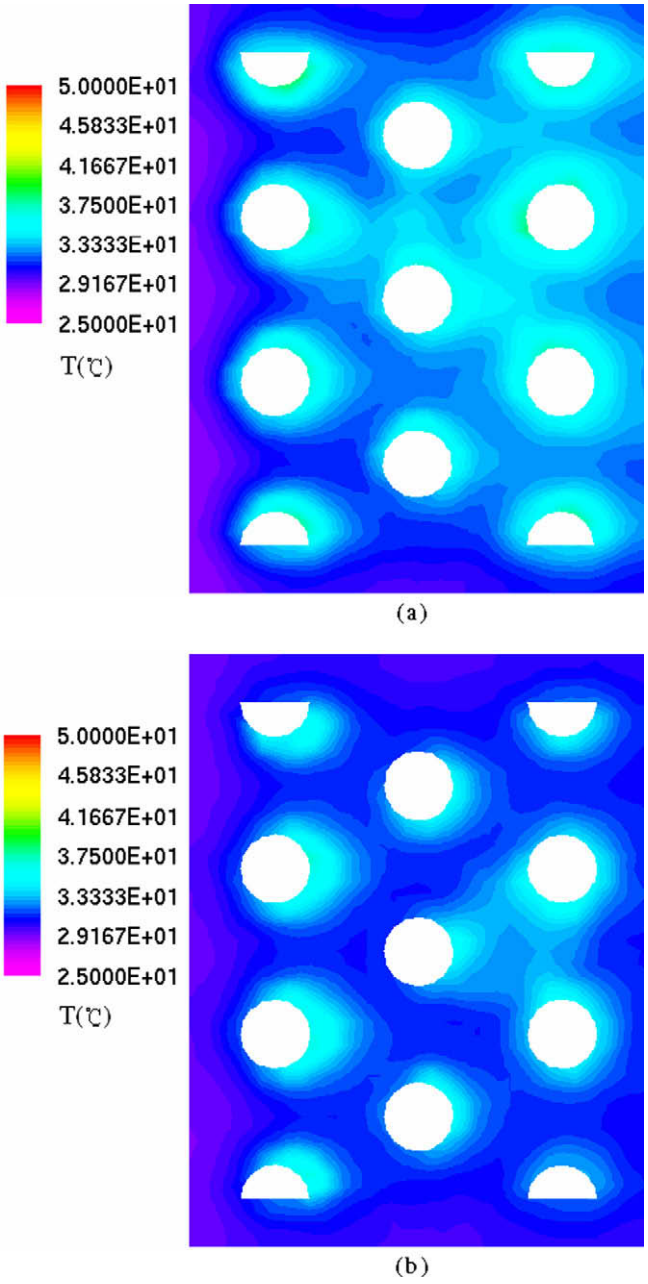

Fig. 11. The measured temperature distributions for the staggered arrangement using U = 1.5 m/s with (a) fp = 10 mm and (b) fp = 15 mm.

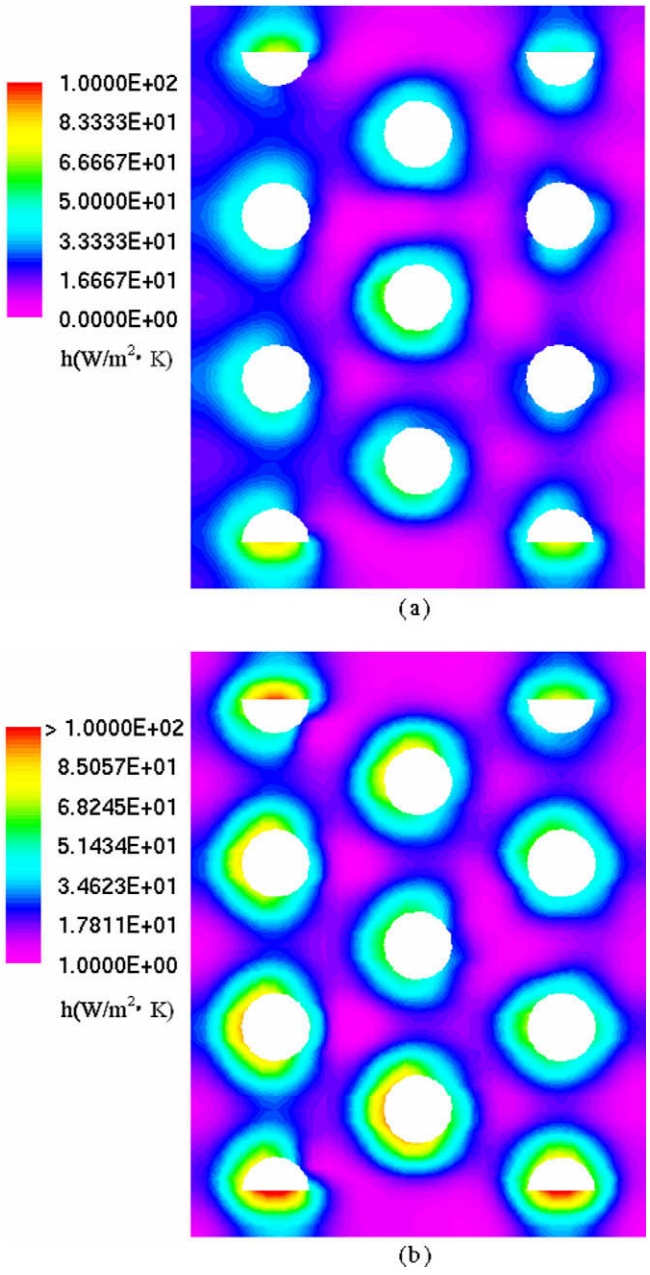

Fig. 12. The estimated heat transfer coefficients for the staggered arrangement using U = 1.5 m/s with (a) fp = 10 mm and (b) fp = 15 mm.

heat exchangers by utilizing the steepest descent method was examined successfully in this work. Two models of fin arrangement with different air velocity and fin pitch were considered. The experimental results show that many interesting phenomena for the local convective heat transfer coefficients have been discovered in the present work and suggested that the staggered tube arrangement is better than the in-line tube arrangement under fixed air velocity and fin pitch conditions since higher heat transfer coefficients can be obtained. Finally, it is concluded that the steepest descent method does not require a priori information for the functional form of the unknown heat transfer coefficients and the reliable estimations can always be obtained.

Table 3
The estimated results of the present work.

	Fin pitch (mm)	Air velocity (m/s)	$\bar{h}$ (W/m^2 K)	Relative error (%) for the estimated temperatures
In-line	10.0	0.5	12.90	0.96
In-line	10.0	1	16.06	0.83
In-line	10.0	1.5	18.35	0.86
In-line	15.0	0.5	16.25	0.98
In-line	15.0	1	20.08	0.75
In-line	15.0	1.5	23.29	0.75
Staggered	10.0	0.5	13.96	0.77
Staggered	10.0	1	17.56	0.71
Staggered	10.0	1.5	20.62	0.88
Staggered	15.0	0.5	17.63	1.14
Staggered	15.0	1	21.92	1.06
Staggered	15.0	1.5	26.32	1.00

Acknowledgment

This work was supported in part through the National Science Council, ROC, Grant No. NSC-97-2221-E-262-MY3.

References

[1] W.M. Kays, A.L. London, Compact Heat Exchangers, third ed., McGraw-Hill, New York, 1984.
[2] G. Cardone, T. Astarita, G.M. Carlomagno, IR heat transfer measurements on a rotating disk, in: D. Balageas, G. Busse, G.M. Carlomagno (Eds.), QIRT 94, Eurotherm Series 42, EETI, 1994.
[3] A. Henckels, F. Maurer, H. Olivier, H. Grönig, Fast temperature measurement by infrared line scanning in a hypersonic shock tunnel, Exp. Fluids 9 (1990) 298–300.
[4] G. Simeonides, P. Van Lierde, S. Van der Stichele, D. Capriotti, J. F. Wendt, Infrared thermography in blowdown and intermittent hypersonic facilities, AIAA Paper 89-0042, 1989.
[5] H. Ay, Heat Transfer and Life of Cutting Tool in Turning, Ph.D. Thesis, University of Michigan, Ann Arbor, MI, 1995.
[6] H. Ay, W.-J. Yang, Heat transfer and life of metal cutting tools in turning, Int. J. Heat Mass Transfer 22 (3) (1998) 613–623.
[7] D.G. Rich, The effect of fin spacing on the heat transfer and friction performance of multi-row plate fin-and-tube heat exchangers, ASHRAE Trans. 17 (1973) 137–145.
[8] D.G. Rich, The effect of the number of tube rows on the heat transfer performance of smooth plate and fin-and-tube heat exchangers, ASHRAE Trans. 81 (1975) 307–317.
[9] F.E.M. Saboya, E.M. Sparrow, Local and average transfer coefficients for one-row plate fin and tube heat exchanger configurations, ASME J. Heat Transfer 96 (1974) 265–272.
[10] F.E.M. Saboya, E.M. Sparrow, Transfer characteristics of two row plate fin and tube heat exchanger configurations, Int. J. Heat Mass Transfer 19 (1976) 41–49.
[11] F.E.M. Saboya, E.M. Sparrow, Experiments on a three-row fin and tube heat exchanger, J. Heat Transfer 19 (1976) 26–34.
[12] F.C. McQusiston, Correlation for heat, mass and momentum transport coefficients for plate-fin-tube heat transfer surfaces with staggered tube, ASHRAE Trans. 84 (1978) 294–309.
[13] H. Ay, J.Y. Jang, J.N. Yeh, Local heat transfer measurements of plate finned-tube heat exchangers by infrared thermography, Int. J. Heat Mass Transfer 45 (2002) 4069–4078.
[14] C.H. Huang, I.C. Yuan, Herchang Ay, A three-dimensional inverse problem in imaging the local heat transfer coefficients for plate finned-tube heat exchangers, Int. J. Heat Mass Transfer 46 (2003) 3629–3638.
[15] W.M. Yan, R.C. Hsieh, C.Y. Soong, Experimental study of surface-mounted obstacle effects on heat transfer enhancement by using transient liquid crystal thermograph, J. Heat Transfer, Trans. ASME 124 (2002) 762–769.
[16] C.H. Huang, H.C. Lo, A three-dimensional inverse problem in predicting the heat fluxes distribution in the cutting tools, Numer. Heat Transfer A 48 (2005) 1009–1034.
[17] C.H. Huang, H.C. Lo, A three-dimensional inverse problem in estimating the internal heat flux of housing for high speed motors, Appl. Therm. Eng. 26 (2006) 1515–1529.
[18] C.H. Huang, L.C. Jan, R. Li, A.J. Shih, A three-dimensional inverse problem in estimating the applied heat flux of a titanium drilling – theoretical and experimental studies, Int. J. Heat Mass Transfer 50 (2007) 3265–3277.
[19] C.H. Huang, M.T. Chaing, A transient three-dimensional inverse geometry problem in estimating the space and time-dependent irregular boundary shapes, Int. J. Heat Mass Transfer 51 (2008) 5238–5246.
[20] O.M. Alifanov, Inverse Heat Transfer Problem, Springer, Berlin, 1994.
[21] CFX-4.4 User's Manual, AEA Technology Plc, Oxfordshire, UK, 2001.